Geoscience Frontiers 14 (2023) 101627

Contents lists available at ScienceDirect

Geoscience Frontiers

journal homepage: www.elsevier.com/locate/gsf

Research Paper

Multi-wing butterfly effects on catastrophic rockslides

Ningsheng Chen [a,b,c], Shufeng Tian [a,d], Fawu Wang [e], Peijun Shi [b,f,*], Lihong Liu [a,g], Miaoyuan Xiao [a,h], Enlong Liu [i], Wenqing Tang [j], Mahfuzur Rahman [k], Marcelo Somos-Valenzuela [l]

[a] Key Lab of Mountain Hazards and Surface Processes, Institute of Mountain Hazards and Environment, Chinese Academy of Sciences, Chengdu 610041, China
[b] Academy of Plateau Science and Sustainability, Xining 810016, China
[c] Kathmandu Center for Research and Education, Chinese Academy of Sciences-Tribhuvan University, Beijing 100101, China
[d] University of Chinese Academy of Sciences, Beijing 100049, China
[e] College of Civil Engineering, Tongji University, Shanghai 200092, China
[f] State Key Laboratory of Surface Processes and Resource Ecology, Beijing Normal University, Beijing 100875, China
[g] Safety Technology Center of Sichuan Bureau of the National Mine Safety Administration, Chengdu 610046, China
[h] Engineering Design & Research Institute of Sichuan University Co.,Ltd, Chengdu 610041, China
[i] State Key Laboratory of Hydraulics and Mountain River Engineering, College of Water Resources and Hydropower, Sichuan University, Chengdu 610065, China
[j] Chengdu Center, China Geological Survey, Chengdu 610081, China
[k] Department of Civil Engineering, International University of Business Agriculture and Technology, Dhaka 1230, Bangladesh
[l] Department of Forest Sciences, Faculty of Agriculture and Environmental Sciences, University of La Frontera, Temuco 4780000, Chile

ARTICLE INFO

Article history:
Received 19 December 2022
Revised 17 February 2023
Accepted 25 April 2023
Available online 29 April 2023
Handling Editor: Wengang Zhang

Keywords:
Catastrophic rockslide
Slope failure
Multi-wing butterfly effect
Tibetan Plateau
Delayed amplified runoff

ABSTRACT

The catastrophic rockslide, which frequently triggers numerous severe disasters worldwide, has drawn much attention globally; however, understanding the initiation mechanism of catastrophic rockslides in the absence of typical single triggering factors related to strong seismic activity or torrential precipitation continues to be challenging within the global scientific community. This study aims to determine the mechanism of the three largest catastrophic rockslides in the eastern Tibetan Plateau, Yigong, Xinmo, and Baige, over the past 20 years using field investigation, remote sensing, and runoff analysis. Instead of the conventional driving factors of heavy rainfall and strong earthquakes, the multi-wing butterfly effects (MWBE) of climatic factors and weak earthquakes are for the first time identified as drivers of the catastrophic rockslide disasters. First, strong tectonic uplift, fast fluvial incision, high-density faults, and large regional water confluence formed the slopes in the critical regime, creating the source conditions of rockslide. Second, the MWBE of early dry-heat events and antecedent rainfall, combined with imminent weak earthquakes, initiated rockslide. Third, the delayed amplified runoff moving toward the sliding surface and lowering the strength of the locking-rock segment constituted the fundamental mechanism of the MWBE on rockslide. The catastrophic rockslide was ultimately inferred to be a nonlinear chaotic process; however, prediction and forecasting of rockslide based on the MWBE in the early stages are possible and essential. This finding presents a new perspective concerning forecasting progressive landslides.

1. Introduction

Landslides cost billions of dollars in damage and claim thousands of lives annually (Handwerger et al., 2016). In particular, high-elevation catastrophic rockslide disasters that have occurred without heavy rainfall or strong earthquakes have drawn significant research attention worldwide (Barnard et al., 2001; Schulz et al., 2009; Coe and J., 2012; Iverson et al., 2015; Watkinson and Hall, 2019). Understanding the mechanism of these rockslide has been a challenging and troubling scientific issue for more than a century.

Globally, catastrophic rockslide disasters without heavy rainfall or strong earthquake occur frequently, particularly in certain regions such as the eastern edge of the Tibetan Plateau, the northwestern edge of the Yunnan Plateau, the Rocky Mountains of North America, the Andes of South America, the Apennines of Central Italy and the European Alps (Delacourt, 2004; Handwerger et al., 2013; Lewkowicz and Way, 2019; Bontemps et al., 2020; Song et al., 2022). These disasters are typically large-scale and tectonically highly complex and frequently occur in the absence of heavy rainfall or strong earthquakes. However, a significant spatiotemporal

* Corresponding author.
E-mail address: spj@bnu.edu.cn (P. Shi).

https://doi.org/10.1016/j.gsf.2023.101627

coupling relationship between the changes in several meteorological factors and weak earthquakes accompanied by these rockslides occurrence can be observed. In 1963, during the analysis of meteorological disasters, the "butterfly effect" was proposed; that is, the phenomenon that a slight change in factors could result in a considerable disaster (Lorenz, 1963; Velasco et al., 2008; Schneider et al., 2010; Ren, 2014; Schwalm et al., 2017; Bloschl et al., 2019). Consequently, we refer to this multi-factor coupling effect as "the multi-wing butterfly effect (MWBE)." The low-frequency characteristics of the MWBE may have a driving impact on landslides similar to that of strong earthquakes or heavy rainfall.

Previous studies have also shown that many natural disasters are caused by multiple factors worldwide (Schulz et al., 2009; Moon et al., 2011; Coe and J., 2012; Larsen and Montgomery, 2012; Watkinson and Hall, 2019; Bontemps et al., 2020). Landslides are caused by the process of slope evolution reaching a critical regime owing to the factors of tectonics, geomorphology, and climate change (Berrocal et al., 1978; Meunier et al., 2008; Carlini et al., 2016; Chen et al., 2019a; Zhang et al., 2022a, 2022b). In addition, extreme climatic conditions and seismic anomalies tend to trigger landslides on slopes that already exist in critical regimes (Keefer, 1984; Moon et al., 2011; Larsen and Montgomery, 2012; Lewkowicz and Way, 2019). The primary causes of catastrophic rockslide disasters are the increase in water pressure and attenuation of rock and soil strength caused by runoff infiltration (Phillips, 1992; Huang et al., 2008; Palmer, 2017; Dille et al., 2022; Gu et al., 2023). Based on this study, we reasonably deduce that rockslide resulted from the increase in water pressure caused by the delay in enlarged runoff infiltration on the slope in the critical regime, owing to the combined effect of low-frequency climatic factors and weak earthquakes. This effect is referred to as MWBE in this study.

The eastern Tibetan Plateau is one of the world's most landslide-prone areas. In 85 years, 52 large landslide disasters occurred in an area covering 60×10^4 km^2 (Supplementary Data Table S1). Six of the 21 largest landslides in the area were catastrophic rockslides without heavy rainfall or strong earthquake. The three largest rocksliedes, Yigong, Baige, and Xinmo, all of which occurred within the past 20 years, were selected for this study. Numerous detailed studies have been carried out for these three rockslides. For Yigong rockslide, tectonic condition (Wang and Lu, 2002), freeze–thaw cycles, glacier melting and heavy rainfall play key roles in the rockslide initiation (Shang et al., 2003; Xu et al., 2012; Zhou et al., 2015). Some researchers have studied the rockslide-dammed lake and outburst flood evolution (Chen et al., 2019b; Turzewski et al., 2020; Zhou et al., 2020). For the Baige rockslide, the coupled effect of exogenic and endogenic factors on landslide occurrence has been explored (Tian et al., 2020; Ding et al., 2021; Yi et al., 2022), the deformation process before the rockslide has been studied by Insar technology (Liu et al., 2020; Xiong et al., 2020; Zhou et al., 2022), and the rockslide-dammed lake and outburst flood evolution conducted was conducted by numerical simulations (Chen et al., 2019b; Ouyang et al., 2019; Wang et al., 2022). For the Xinmo rockslide, the relationship between landslides and historical earthquakes, rainfall in early stage, and river incision has been studied (Fan et al., 2017; Huang et al., 2019), the deformation characteristics were obtained by Insar technology (Dong et al., 2017; Intrieri et al., 2017), and the movement process was studied by numerical simulation (Scaringi et al., 2018; Zhao et al., 2021). However, understanding the initiation mechanism of catastrophic rockslides in the absence of typical single triggering factors related to strong seismic activity or torrential precipitation continues to be challenging within the global scientific community. These three catastrophic rockslides all exhibit large scale, are located at high altitudes and lack significant triggering factors. Furthermore, they have shown clear response to minor meteorological changes and weak earthquakes of the MWBE. Therefore, this study presents optimal prospects for revealing the mechanism of catastrophic rockslides and draws our focus toward the potential general disaster laws of multi-wing rather than single-wing butterfly effects.

2. Methods

First, the inductive methods of multi-type data were used to prove the existence of the phenomenon of the MWBE (Supplementary Data Text S1). The tectonic uplift rates of the catastrophic rockslides areas were determined using the historical global positioning system (GPS) and modern GPS monitoring based on the crustal movement (Liu et al., 2010). The linear fault density was calculated by measuring the fault length in the square with a uniform area of 100 km^2 in the study area. The size, gradient, slope direction, locked segment location, and water confluence area were obtained by analyzing post-sliding field photos, remote sensing imageries, and Google Earth images. The fissure and joint densities and rock orientation were obtained by field investigation. The geotechnical characteristics were obtained by analyzing the rock quality designation (RQD) value of the boreholes and on-site geological exploration. An X-ray diffraction analysis yielded the mineral contents of the weathered materials on the sliding surface.

Second, by understanding the spatial–temporal coupling relationship between deformation and runoff amplification and hysteresis, the MWBE of each rockslide in the critical regime was revealed (Supplementary Data Text S1). Based on multi-site and multi-period meteorological, hydrological, and seismic data, the characteristics of the MWBE of the earthquakes, temperature, and rainfall changes on the catastrophic rockslides were analyzed, and the frequency of the catastrophic rockslides was calculated. The recharged snowmelt of the Yigong rockslide was calculated using the degree-day model, which is based on the linear relationship between ice and snow melting and the positive accumulated temperature (Zhang et al., 2006). The recharged runoff of rockslide was obtained through the soil conservation service curve number (SCS-CN) hydrological model based on the water balance equation. The Slope/W and Seep/W modules in the Canadian geotechnical simulation software GeoStudio were used to analyze the relationship between the externally supplied seepage and the slope stability. This study also explored the relationship between deformation and seepage using the method of lagged correlations (Bevacqua et al., 2021) (supplementary methods). The number of days that landslide deformation lags behind peak runoff is then determined based on the temporal distribution of runoff. Besides, the deformation of the Baige rockslide and Xinmo rockslide was derived from two existing representative studies (Intrieri et al., 2017; Li et al., 2020).

Third, based on the nonlinear theory, the evolution process of the MWBE was corroborated and discussed (Supplementary Data Text S1). The logistic growth model, also known as a self-inhibition equation, was used in this study to analyze the deformation characteristics of the landslide (May 1976; Alsharawi and Angelos, 2006).

The following logistics difference Eq. (1) was used in this study:

$$\frac{dX_n}{dt} = kX_n(1 - X_n) \tag{1}$$

where k denotes the growth rate of the deformation rate (x_{n+1}) at a certain time relative to the deformation rate (x_n) of the previous period, and X_{n+1}, X_n represents the ratio of x_{n+1}, x_n to the maximum deformation of the existing slopes. When k is < 1, the landslide is in the normal creep stage; when k is between 1 and 3, the landslide is

in the accelerated deformation stage, and when k is > 3 the landslide is assumed (predicted).

3. Results

3.1. Large scale and long cascade characteristics of catastrophic rockslide disasters

In 2000–2019, the Yigong, Baige, and Xinmo catastrophic rockslides occurred within deep-cut canyons of the Yigong Zangbo River (the tributary of the Yarlung Zangbo River), the mainstream of the Jinsha River, and Songping gully (the tributary of the Minjiang River), respectively, in the eastern mountainous area of the Eastern Tectonic Syntaxis of the Tibetan Plateau. The three rockslide disaster chains are located respectively on the northern edge of the Eastern Tectonic Syntaxis, the suture zone of the Jinsha River, and the western edge of the Minjiang Fault block (Fig. 1a). The elevations of the shear outlets of all three rockslide disasters exceed 3047 m, with the highest being the Yigong rockslide at 4510 m. Thus, they are identified as high-elevation catastrophic rockslides that formed long disaster chains and resulted in large volumes of altered materials. The volumes of the Yigong, Baige, and Xinmo rockslides were 199, 22, and 8 million m^3, respectively (Supplementary Data Figs. S1–S5, and Supplementary Data Table S2). The first rockslide, Yigong, dammed the Yigong Zangbo River and breached the resulting barrier lake, causing flooding at a peak discharge of 100,000 m^3/s (Chen et al., 2019b). This resulted in a 606-km-long disaster chain with economic losses amounting to 294.42 million dollars in China and approximately 94 casualties in India (Fig. 1a, Supplementary Data Table S3). The second rockslide, Baige, was not fatal, owing to successful intervention and

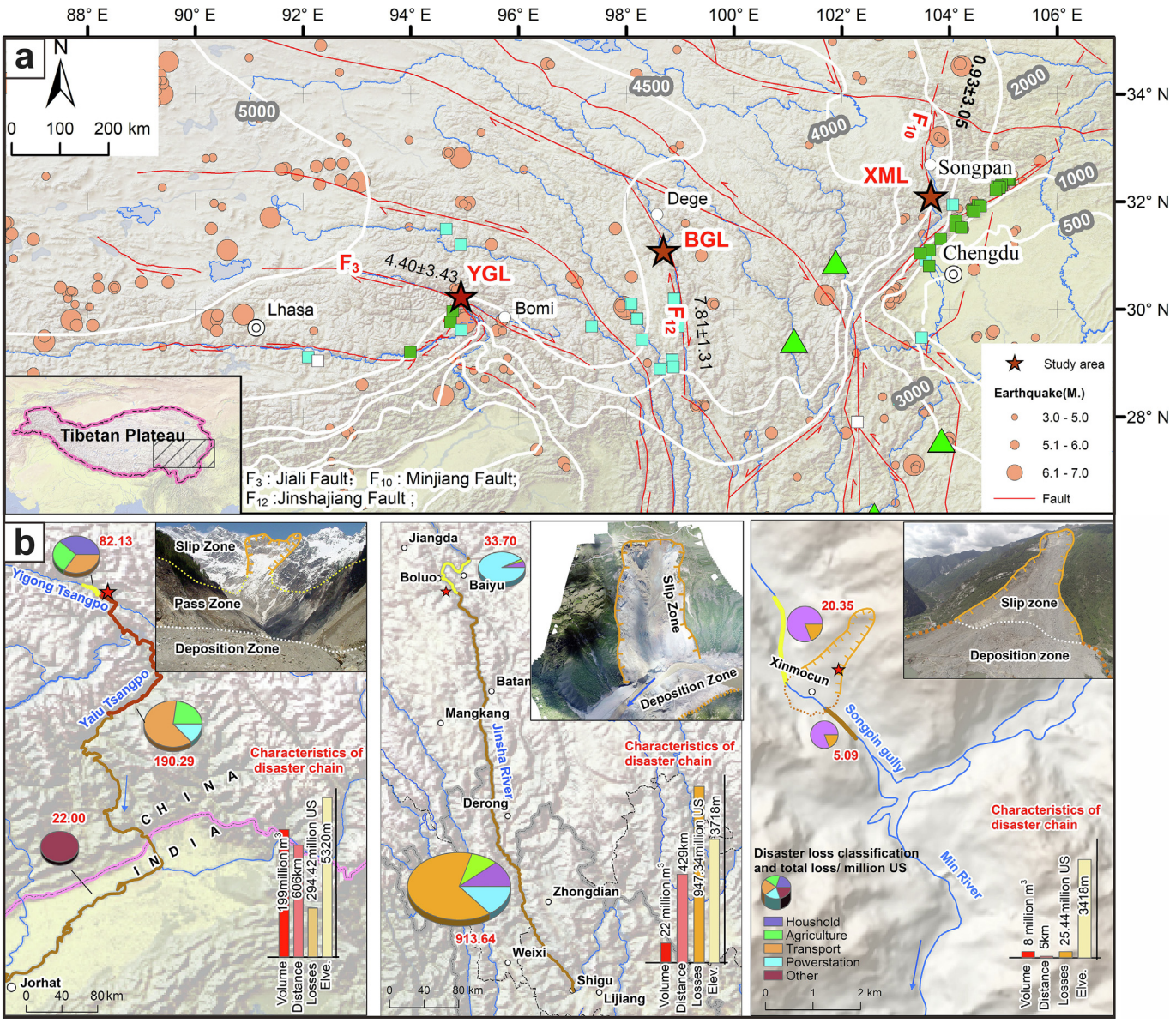

Fig. 1. Map and geographical setting of the three catastrophic rockslides in the eastern Tibetan Plateau. (a) Location map of the study area. The red, white, and yellow lines represent the fault, contour, and topographic profile. Circles of different sizes indicate earthquakes of different magnitudes ($M_s > 4.3$). Blue, green, and white squares represent the large landslides caused by heavy rainfall, earthquake, and human activities, respectively (Supplementary Data Table S1). The green triangle represents catastrophic rockslides without heavy rainfall or strong earthquake before 2000. The red five-pointed stars indicate the locations of the three catastrophic rockslides within the last 20 years. YGL: Yigong rockslide, BGL: Baige rockslide, XML: Xinmo rockslide. (b) The scale of the three catastrophic rockslides disasters and resulting losses. (For interpretation of the references to colour in this figure legend, the reader is referred to the web version of this article.)

forewarning. However, the flood resulting from the barrier lake breach at a peak discharge of 31,000 m^3/s (Fan et al., 2019b) caused economic losses of 947.34 million dollars and a 429 km-long disaster chain (Fig. 1b). The third rockslide, Xinmo, resulted in 83 casualties, financial losses amounting to 25.44 million dollars, and a disaster chain>5 km in length (Fig. 1c, Supplementary Data Tables S3, S4, and S5).

3.2. Catastrophic rockslides occurred in critical slopes formed in a unique geological and geomorphic environment on spatial scale

The stability analysis results revealed that the safety factor of the three rockslides before severe deformation varied between 1.09 and 1.25, which highlights the slope characteristics of the critical regime. Evidently, the three catastrophic rockslide areas featured the characteristics of high fault density, strong tectonic uplift, fast fluvial incision, a high and steep slope, low rock strength, and a weak sliding face (Fig. 2). The fault lengths in the area within 100 km^2 of the landslides were 30.1, 29.9, and 33.9 km for the Yigong, Baige, and Xinmo rockslides, respectively. Correspondingly, the fault densities were 2.3, 1.6, and 9.6 times the density of the regional average faults (Supplementary Data Fig. S6). Meanwhile, all three rockslides are located in areas with strong tectonic uplift. From lowest to highest, the uplift rates in the Xinmo, Baige, and Yigong rockslide areas were observed to be 1.9, 4.0–6.0, and 12.9–14.1 mm/yr, respectively (Supplementary Data Table S6 and Figs. S7, S8). Between all the three catastrophic rockslides, a high elevation difference is exhibited, between 810 m and 1300 m, with slopes ranging of 29°–40°.

Meanwhile, the rock mass of all slopes in the critical regime has been severely weathered, thereby exhibiting a broken structure. The sloping rock has formed fracture zones with thicknesses ranging of 50–90 m. The joint fissures of the rock are also well-developed, producing three groups of joints and thereby segmenting the rock into broken blocks with joint fissure densities ranging of 7–10 pieces/m (Supplementary Data Fig. S9). The bedrock at all sites has undergone severe chemical weathering, amplified by the runoff from in the watershed adjacent. For the Baige rockslide, serpentinite weathering has formed clay minerals with a small amount of calcitic cementation. In the serpentinite, 49% lizardite (H, Mg, O, and Si), 39% chrysotile (H, Mg, O, and Si), 9% dolomite (C, Ca, Mg, and O), 3% magnetite, and 1% calcite were observed (Supplementary Data Fig. S10). The weathered soil of the Xinmo rockslide sliding surface contained 30.9%, 30.6%, 28.5%, 9.0%, and 0.9% of mica, quartz, feldspar, chlorite, and magnetite contents, respectively. The clay mineral content in the deposition area of the Yigong rockslide was 3.2%.

For all sites, the prolonged geological processes lead to a weak sliding surface on the slope in the critical regime subject to the supporting force of a locked segment. The sliding surface after the rockslide comprised a smooth sliding surface and a new brittle fracture surface (Supplementary Data Fig. S11). For the Xinmo rockslide, the upper part of the sliding surface comprised a strong weathered surface that appeared to have formed over a relatively long period of geological history, with an average length of 414 m, a width of 231 m, and an orientation of 196°∠40° (dip direction∠ dip angle) (Supplementary Data Fig. S11). The orientation, average length, width, and thickness of the lower section

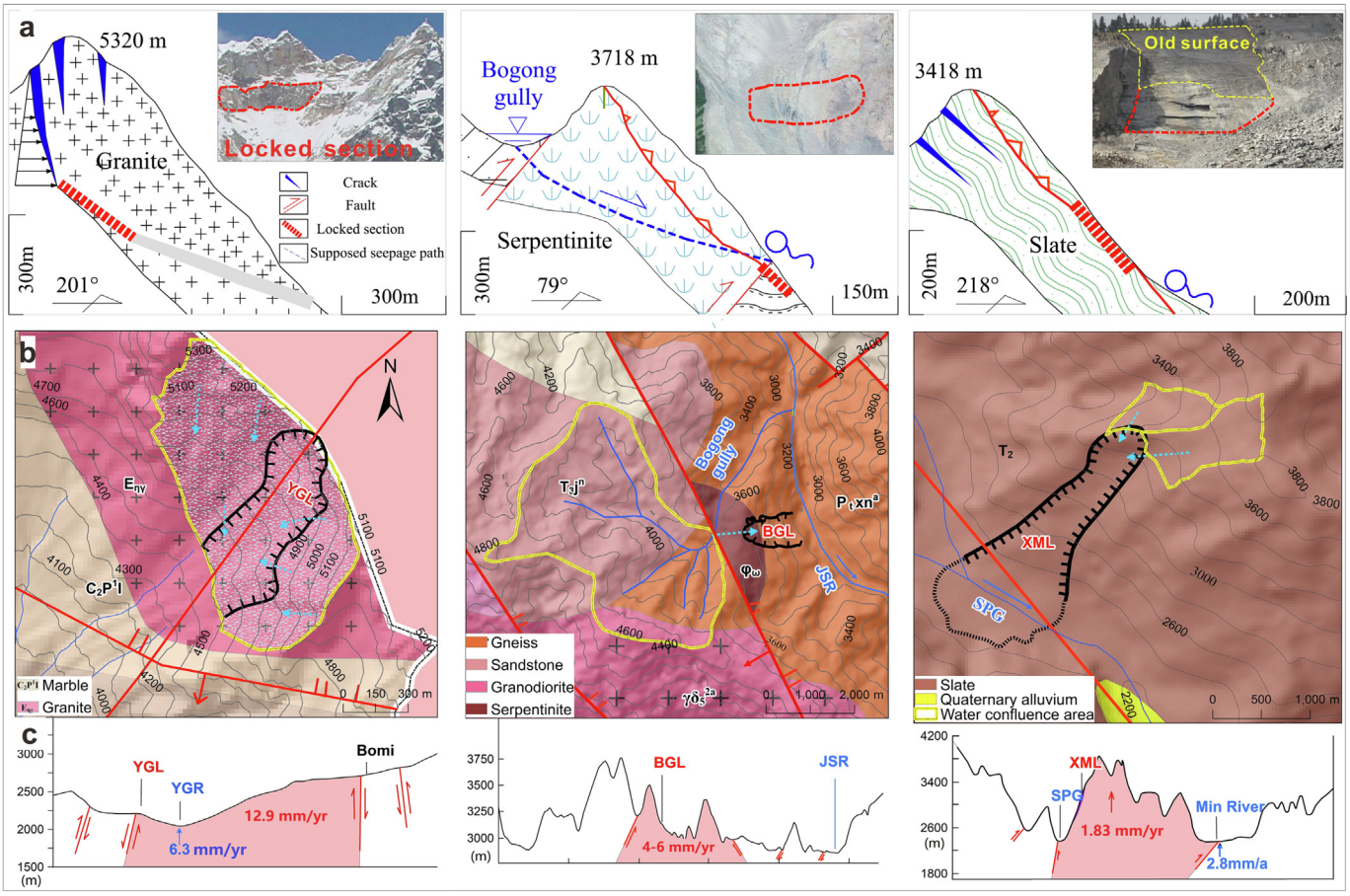

Fig. 2. Slope in the critical regime of the three catastrophic rockslides and the geological and geomorphological background. (a) Schematics of Yigong, Baige, and Xinmo rockslides. (b) Geological and geomorphological maps of the Yigong, Baige, and Xinmo rockslides. (c) Geological profiles of the Yigong, Baige, and Xinmo rockslides.

are 217°∠33°, 181 m, 136 m, and 61 m, respectively. For the Baige rockslide, a weak sliding surface with a length of 950 m and an average width of 290 m developed on the slope surface that appeared following the landslide itself. A new locked segment of metamorphic gneiss with a length of 199 m outcropped at the lower part of the sliding surface. For the Yigong rockslide, a locked segment with a length of 206 m developed in the middle of the landslide surface within an altitude ranging of 4551–4697 m, forming a new fractured section. The sliding surface of the Yigong rockslide was formed along with two sets of south-dipping joints. The top and bottom parts of the sliding surface are connected, with the top at the altitudes of 5320–4697 m and the bottom at 4551–4510 m (Supplementary Data Fig. S12).

3.3. The MWBE of multiple meteorological and earthquake factors on catastrophic rockslides in temporal scale

Notably, only one earthquake with a magnitude of 4.8 occurred before the Yigong rockslide. Based on the intensity–duration (I–D) model (Copernicus, 2020), the minimum rainfall intensities over 24 h required to induce the Yigong, Baige, and Xinmo rockslides were 3.5, 2.4, and 2.2 mm/h, respectively. However, the actual precipitation levels were much lower, at 0.47, 0.00, and 0.94 mm/h, respectively. Therefore, the imminent short-term rainfall is unlikely to have solely induced the catastrophic rockslides (Supplementary Data Fig. S13).

Overall, the catastrophic rockslide occurrences exhibit temporal coupling with the MWBE of early dry-heat events, antecedent rainfall, and imminent earthquakes. These processes show the characteristics of the MWBE to have a low superposition frequency (once in 1203–3922 years). For the Yigong rockslide, the driving factor was the MWBE of climatic factors and weak earthquake (Fig. 3a). In 2000, this Yigong rockslide was influenced by a dry-heat event during winter and spring and an imminent earthquake with a magnitude of 4.8. The standard precipitation index (SPI) in February 2000 was −1.67, with a low frequency of 0.05, indicating a severely dry state before the rockslide. In addition, a remarkable increase in temperature occurred from April 1 to April 9, 2000, with an average temperature of 4.63 °C and a low frequency of 0.075. The earthquake acceleration generated at the rockslide location by the imminent small earthquake on April 9, 2000, was 43.32 Gal, with a low frequency of 0.1522. Before the Yigong rockslide, the cumulative rainfall from January 1 to April 9, 2000, was 107.9 mm, less than the average precipitation over the same period, and the frequency was 0.6744. The superposition frequency of the Yigong rockslide indicators was determined to be once in 2598 years (Supplementary Data Table S7). For the Baige rockslide, the driving factor was the MWBE of antecedent rainfall and increasing winter and spring temperatures (Fig. 3b). In 2018, this rockslide occurred under extreme antecedent rainfall and dry heat during winter and spring. The lowest temperature from March to May 2018 was −1.2 °C, and the frequency was as low as 0.0172. The cumulative antecedent rainfall from July 01 to October 10, 2018, was 530.2 mm, and the frequency was as low as 0.0323. The lowest SPI during the winter and spring before the rockslide was −0.4, which was close to the average SPI in the same period, and the frequency was 0.459. Therefore, the superposition frequency of the Baige rockslide indicators was determined to be once in 3922 years (Supplementary Data Table S7). For the Xinmo rockslide, the driving factor was the MWBE of antecedent rainfall and the dry-heat event during winter and spring (Fig. 3c). In 2017, it occurred under extreme dry heat during winter and spring, along with antecedent rainfall. The lowest SPI before the rockslide was −1.61 in January 2017, and the frequency was as low as 0.1364, indicating that conditions were severely dry before the rockslide. The average lowest temperature during winter and spring, from March to May 2017, was −1.8 °C, and the frequency was as low as 0.0408. The cumulative antecedent rainfall from March 1 to June 24, 2017, before the Xinmo rockslide, was 342.9 mm, and the frequency was as low as 0.1493. Therefore, the superposition frequency of the Xinmo rockslide indicators was determined to be once in 1203 years (Supplementary Data Table S7).

3.4. Enlarged lagging runoff driving mechanism of the MWBE on catastrophic rockslides

Owing to the MWBE, either the amplified and delayed runoff or the additional influence of imminent earthquakes increased the water pressure, thereby promoting the rupture mechanism of the locked segment and triggering the occurrence of rockslide. In terms of geomorphology, the formation area of an rockslides generally includes an additional water confluence area of 4.9–23.9 times the landslide area and can be categorized into three models: the slope, valley, and ice melting models (Fig. 2b). For the Baige rockslide, the valley infiltration of the watershed (14.8 km^2) at the sloping rear increased the seepage of the landslide (Fig. 2b). The additional water confluence catchment area was 23.9 times more than the landslide body above the locked segment. For the Yigong rockslide, an ice–snow meltwater confluence area of 1.12 km^2 was observed around the landslide body, 4.9 times that of the landslide body above the locked segment (Fig. 2b). For the Xinmo rockslide, the runoff water on the sloping rear and the lateral confluence water infiltrated the landslide slope along the bedding plane and fissures. The water replenishment area of the Xinmo rockslide was 0.84 km^2, which is 5.6 times that of the landslide body above the locked segment (Fig. 2b). Also, the groundwater has become exposed at the front edge of the landslide. The slope of the rockslides typically exhibited a replenishment effect of runoff amplification caused by the landforms from the exterior of the body of each rockslide. The runoff amplification caused by the combination of antecedent rainfall, antecedent temperature, and the confluence of the landforms significantly increased the seepage rate of the slope, which was 8.5–26 times more than that of the body of the landslides (Fig. 3d, e, f). For the Baige rockslide, the maximum seepage rate from the landslide body was 0.1 m^3/s on July 2, 2018, whereas that from the Bogong gully at the rear of the landslide was 2.6 m^3/s, 26 times more than that of the body of the slope. For the Xinmo rockslide, the maximum seepage rate from the landslide body was 0.01 m^3/s on June 1, 2017, whereas that from the rear and lateral side of the slope was 0.1 m^3/s, which is ten times more than that of the body of the slope. For the Yigong rockslide area, the precipitation from April 1–9, 2000, was 42.9 mm, and the amount of snowmelt was 288.2 mm. The maximum daily average discharge was 1.07 m^3/s on April 1, 2000, entirely generated by snowmelt. The runoff generated by snowmelt was 8.5 times more than that caused by precipitation.

Many studies analyzed the deformation characteristics of the rockslide based on remote sensing techniques, such as time-series SAR observations, and found that both the Xinmo rockslide and the Baige rockslide had a long history of deformation (Intrieri et al., 2017; Li et al., 2020). In particular, the cumulative deformation of the Baige landslide was as much as 40 m in the past decade before the event (Fan et al., 2019a). In addition, significantly accelerated deformation phases were detected before the landslides occurred. However, there was no heavy rainfall or strong strong earthquakes at the time of landslide occurrence. From these results, it can be stated that the long-distance infiltration of enlarged runoff causes significant hysteresis of landslide occurrence. For the Baige rockslide, based on the lagged correlation analysis, the correlation coefficient between landslide deformation and seepage was highest when deformation lagged seepage by 88–91 days, with 0.87–0.92 (Fig. 3e and Supplementary Data

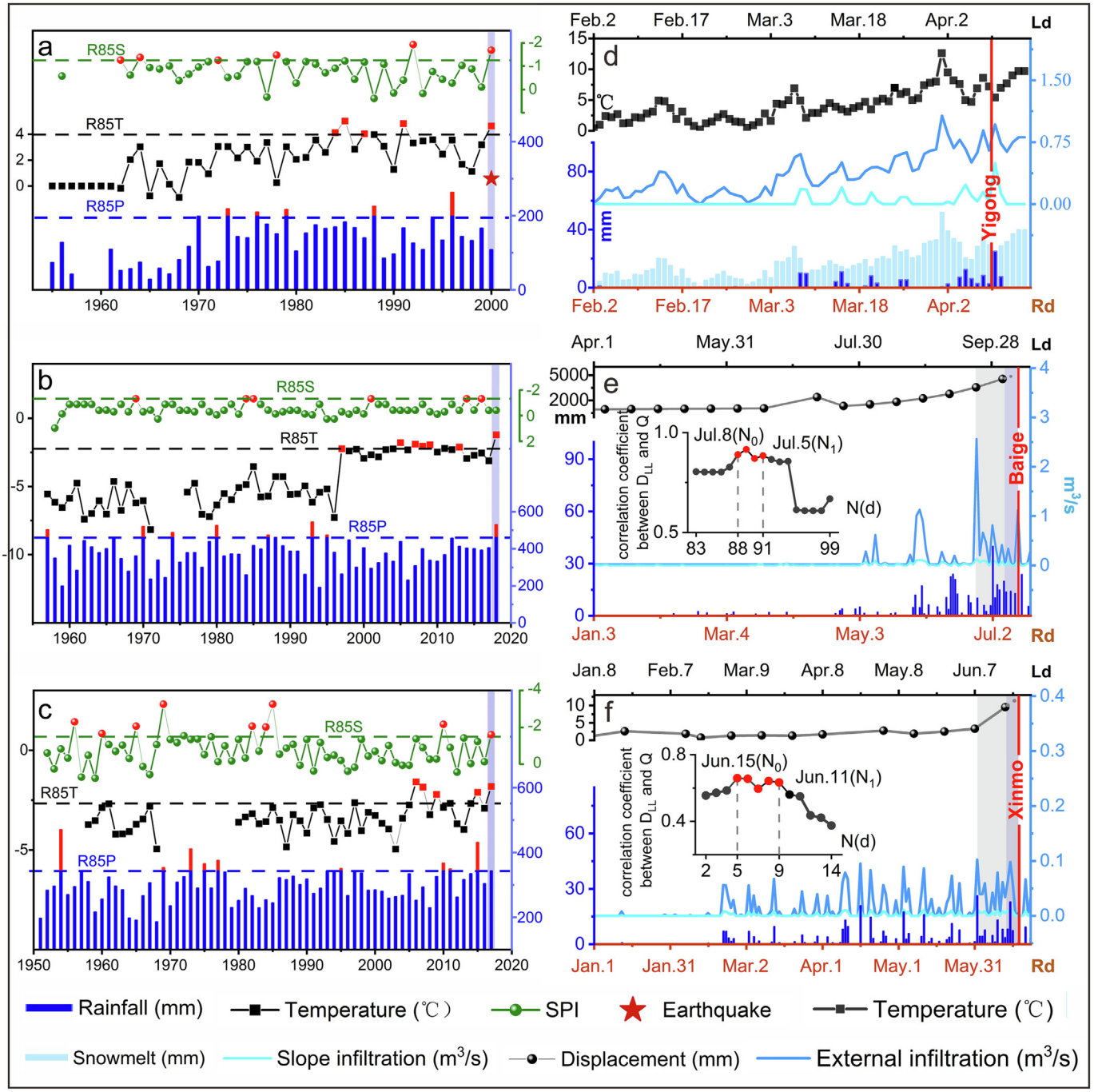

Fig. 3. The multi-wing butterfly effect (MWBE) of early dry-heat events and antecedent rainfall, combined with imminent weak earthquakes and enlarged lagging runoff, promoted the deformation and catastrophic rockslides. R85S, R85T, and R85P represent the 85th percentile line of drought, temperature, and antecedent rainfall during the same period of all recorded years, respectively. DLL means landslide deformation (adapted from Intrieri et al. (2017); Li et al. (2020)), and Q represents the infiltration rate. Rd and Ld represent runoff data and landslide data. (a) The MWBE of an imminent earthquake, increasing temperature, and severe drought for the Yigong rockslide. (b) The MWBE of antecedent rainfall and rising temperature for the Baige rockslide. (c) The MWBE of antecedent rainfall, increasing temperature, and severe drought for the Xinmo rockslide. (d) The plot of the surface runoff of the Yigong rockslide from snowmelt and rainfall was 8.5 times more than the surface runoff from only rainfall. (e) The plot of the seepage rate of the Baige rockslide from Bogong gully, which was 26.0 times that from the body of the slope, and the possible time for the deformation to lag precipitation was 88–91 d. (f) The plot of the seepage rate of the Xinmo rockslide, which from the rear and lateral sides, was ten times more than that from the slope body, and the possible time for the deformation to lag precipitation was 5–9 d.

Fig. S14a). So the seepage discharge from June 26 to July 7, 2018, was found to have caused the most considerable deformation of 455.1 cm from September 22 to October 3, 2018, and the deformation lagged 89 days after the date of the maximum seepage. Therefore, for the Baige rockslide, it can be concluded that the maximum seepage from the Bogong gully, which occurred 89 days earlier, caused the most considerable deformation on October 3, 2018. Following this, the continuous heavy rainfall of 41.0 mm in the subsequent six days (July 8–13) led to the rockslide occurrence on October 10, 2018 (Fig. 3e). For the Xinmo rockslide, based on the lagged correlation analysis, the correlation coefficient between landslide deformation and seepage was highest when deformation lagged seepage by 5–9 days, with 0.60–0.66 (Fig. 3f and Supplementary Data Fig. S14b). So, the seepage discharge of June 1–12,

2017, resulted in a maximum deformation of 9.5 mm during June 8–19, 2017. The deformation lagged eight days after the date of the maximum seepage. Therefore, the maximum seepage of the Xinmo rockslide that occurred eight days earlier caused the largest deformation. The continuous rainfall of 39.1 mm in the subsequent five days (June 13–17, 2017) led to the rockslide occurrence on June 24, 2017 (Fig. 3f). For the Yigong rockslide, the extremely high temperature (1955–2018, T95P > 95%) that occurred nine days before the landslide caused maximum snowmelt runoff. The snowmelt runoff most likely infiltrated and reached the locked segment after nine days, thereby initiating the landslide (Fig. 3d). The delayed and enlarged runoff led to an increase in water pressure, consequently reducing the strength of the locked segment. Numerical simulation results reveal that the initial water pressures of locked segments in the Yigong, Baige and Xinmo rockslides were −14.95, 56.02, and 19.64 kPa, respectively (Supplementary Data Figs. S15, S16, S17, and Table S8). Moreover, the internal and external geological dynamic effects decreased the strength of the locked segments by 0.28–0.77 times that of their initial regimes. For all the rockslides, the replenishment runoff increased the water pressures of the locked segments in Yigong, Baige, and Xinmo to 140.21, 118.81, and 1608.21 kPa at the time of each landslide, which was 10.37, 2.12, and 81.88 times more than the initial water pressures, respectively. The continuous increase in water pressure and decrease in rock mass strength at all sites eventually led to the rockslides. In addition, for the Yigong rockslide, a small earthquake before the landslide further increased the water pressure and promoted the landslide at that site.

3.5. Formation processes of MWBE on catastrophic rockslides

The formation of these catastrophic rockslide is a chaotic slope process in the critical regime subject to the MWBE events and can be predicted early in the process. For any given rockslide where a fractured weathering face and locked segment with low weathering intensity co-exist, the sliding face is non-homogeneous, and the evolution process is nonlinear. The loose deposits heaped at the toe of the slope after the occurrence of rockslide show us the chaotic system existence. The slope in the critical regime formed by tectonics and climate change in the early stage of the landslide process indicates the starting location for the evolution of the chaotic system. The fractured surface of the locked segment in the body of the landslide reflects characteristics of the micro-fracture process of the rock, in which a thermodynamic entropy reduction process occurs, thereby indicating one stage of the chaotic process. Many factors, such as early-micro disturbances, pro-micro disturbances, and imminent micro-disturbances of the rockslide, jointly play a role in the specific mode of the event (Fig. 4). Changes in temperature and antecedent rainfall and drought combined with or without earthquakes amplify exceptional runoff and can also cause considerable disturbances to a landslide. The complexity of these factors demonstrates that catastrophic rockslide is a chaotic process. Further, the deformation process of rockslide is positively affected by the increase in water pressure and the decrease in resistance caused by the runoff infiltration. Meanwhile, deformation is negatively affected by the leakage, evaporation, and consolidation of the sliding surface. For example, the maximum Lyapunov exponents of the Xinmo and Baige rockslides were found to be 0.1329 and 0.0771, respectively (Supplementary Data Fig. S18). In this way, the rockslide deformation process satisfies the chaotic process of the logistics difference equation.

The ratios of the last recorded deformation velocity to the previous deformation velocity before the Xinmo and Baige rockslides were 2.88 and 1.28, respectively. They were consistent with the characteristics of the balance section of the logistics difference equation. As shown in Fig. 4, the entire deformation process of rockslide can be divided into the normal creep deformation phase (k < 1), accelerated deformation phase (k = 1 to 3), and chaotic phase of rupture and sliding of a locked segment (k > 3). In the normal creep deformation phase, the negative effect is greater than the positive effect. In the sliding phase, the positive impact is significantly greater than the negative effect, and the slope begins to enter a chaotic process. In the accelerated deformation phase, the rockslide process with a k value ranging from 1 to 3 can be predicted and forewarned about.

4. Discussion

Based on the aforementioned research, the MWBE mechanism of catastrophic rockslides is considered universally applicable. According to the disaster data published in the China Geological Environment Bulletin and the China Geological Survey, 502 catastrophic rainfall-induced landslides with casualties or property losses of >1 million RMB occurred in China between 2010 and 2020. Among them, at the occurrence time of 340 landslides (accounting for 67.9% of the total), there was no heavy rainfall or strong earthquakes that could be said to have directly triggered these landslides. Instead, the landslides were mainly affected by multiple other factors such as antecedent rainfall, dry-wet cycles and freeze–thaw cycles at early stages, light-to-moderate seismic shaking, and landform runoff amplification (Shang et al., 2003; Gariano and Guzzetti, 2016; Su et al., 2017; Tian et al., 2020; Song et al., 2022). Similarly, precipitation clustering was detected before 83% of landslides in Portugal (Bevacqua et al., 2021). These show that the MWBE has a universal influence on landslides. In addition, indications of MWBEs can be noted from typical cases of large-scale landslide disasters, such as the Lugong and Touzhai landslides on the Yunnan–Guizhou Plateau in China, the Tanggudong landslide on the eastern edge of the Tibetan Plateau in China (Huang, 2009), the Peruvian Mantaro landslide in the Andes (Berrocal et al., 1978), and the Honduran EI Berrinche landslide (Olsen and Villanueva, 2007).

Moreover, most debris flow disasters related to landslides are also the result of MWBE. For example, in the Panxi region of China, only about 40% of debris flows and heavy rainfall occur simultaneously (Tan et al., 1994). Thus, it is reasonable to infer that 60% of debris flow disasters are related to the effects of multi-factors, such as antecedent rainfall and dry-wet and freeze–thaw cycles. In addition, according to the 3839 catastrophic debris flows in Sichuan Province, China from 1949 to 2017 the distribution of debris flows showed that 90% were distributed in dry valleys and seismic zones (Di et al., 2019). This phenomenon indicates that the distribution of debris flows is not only controlled by rainfall but also by the characteristics of soil masses, topography, and other factors in dry valleys and seismic zones. Based on this, debris flows are clearly the result of multiple factors, that is, the MWBE described in this paper. For example, the Zhouqu debris flow that occurred on August 8, 2010, was affected by numerous factors, such as drought, which caused soil cracking, disturbances from the Wenchuan earthquake in its early stages, heavy rainfall, and human activities (Ren, 2014). The drought before the Puge debris flow, which occurred on August 8, 2017, was also conducive to the occurrence of debris flow (Zhong et al., 2021).

The aforementioned landslides and debris flows are examples of the extreme process of gravitational erosion in the evolution of landforms (Egholm et al., 2013). Geological disasters such as landslides and debris flows can be induced by heavy rainfall or strong earthquakes and can also be caused by MWBE. There are differences between the landslides caused by MWBE and the landslides induced by strong earthquakes or heavy rainfall (Table 1). How-

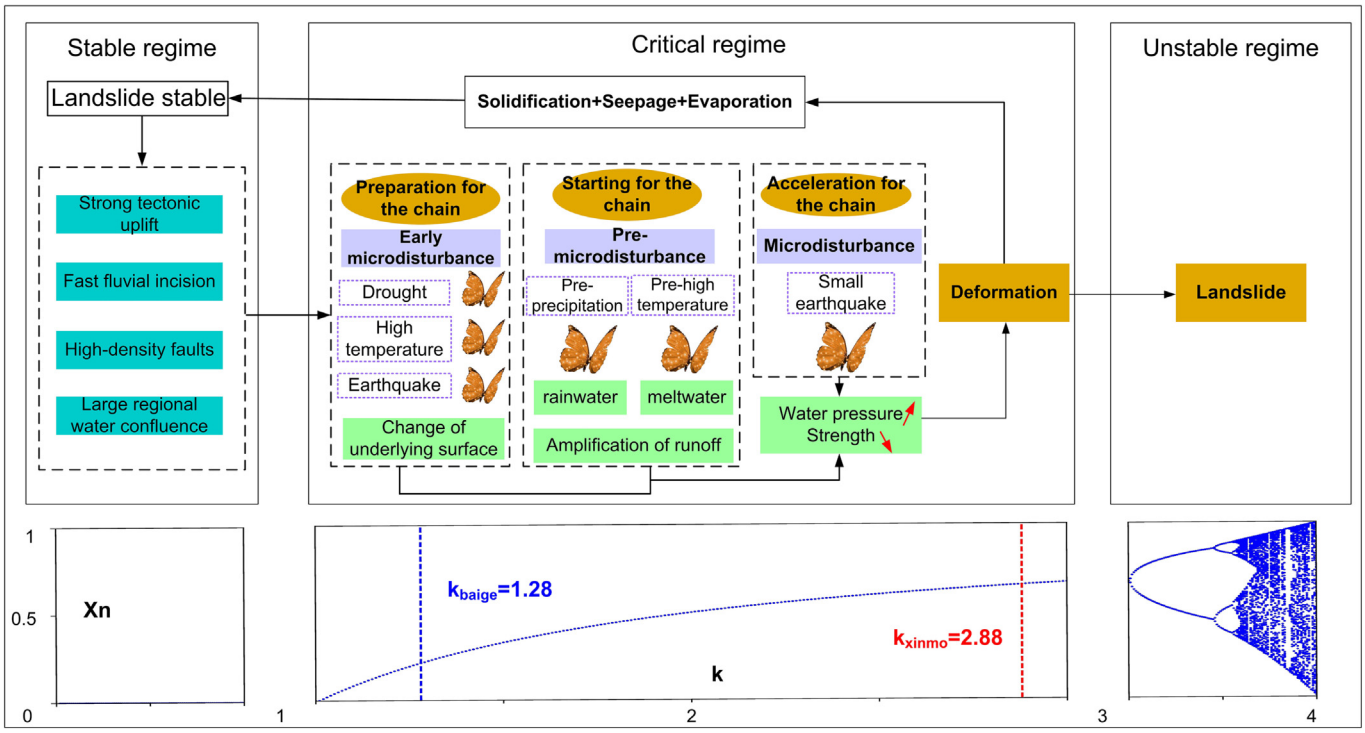

Fig. 4. Schematic of the MWBE-based chaotic structure of catastrophic rockslides. The value of k denotes the growth rate of the deformation rate within a certain period relative to the deformation rate of the previous period. At the same time, X_n represents the ratio of deformation rate to the maximum deformation of the existing slopes within a certain period. The solid blue line comes from the logistics difference equation. The blue and red dotted lines represent the k values of Xinmo rockslide and Baige rockslide, respectively. (For interpretation of the references to colour in this figure legend, the reader is referred to the web version of this article.)

Table 1
Main differences between the landslides caused by MWBE and the landslides induced by strong earthquakes or heavy rainfall.

	Landslides induced by MWBE	Landslides induced by strong earthquakes	Landslides induced by heavy rainfall
Drivers	Compound of multiple drivers	Strong earthquakes	Heavy rainfall
Distribution	Individual distribution	Strip-like distribution	Regional distribution
Scale	Very large scale, mainly deep landslides	From very large to small scale	Moderate or small scale, mainly shallow landslides
Time	Spring or Summer or Fall	/	Mainly during Summer
Preconditions	Slope in critical regime with weak-soil and strong-water conditions	/	/
Mechanism	Increased water pressure caused by amplified and delayed runoff	Reduction of elastic modulus, the formation or widening of cracks at the top of the slope, etc.	Increase in soil water content, pore water pressure, and buoyancy force
Prediction and warning	Combination of rainfall trends, topographic features, the compound of multiple drivers, and deformation indicators	Synchronization with prediction and warning of strong earthquakes	IntensityDuration curve and deformation indicators

ever, consider that the energy accumulation process of a strong earthquake with a magnitude of 8 or above, such as the Wenchuan earthquake, takes about 4000 years (Shen et al., 2009). Meanwhile, super-heavy rainfall, which can directly trigger landslides and debris flows, tends to be a low-frequency event, usually once in a hundred years to once in a thousand years (Huang, 2009). The MWBEs analyzed in this study are also low-frequency events representing the combination of early extreme drought, temperature changes, antecedent rainfall, and weak earthquakes. Therefore, the MWBE is a widespread condition that can cause landslides and debris flows in long-term landform evolution.

In summary, the proposed MWBE mechanism for catastrophic rockslides reflects that low-frequency events involving multiple small factors can be an alternative for the role of a single highly abnormal earthquake or heavy rainfall as the triggers of catastrophic landslides/rockslides. Besides, the MWBEs formed by combining multiple factors are universal.

5. Conclusions

Using the three largest rockslides (Yigong, Xinmo, and Baige) in the eastern Tibetan Plateau over the past 20 years as a basis, this paper proposes for the first time that the multi-wing butterfly effects (MWBE) of climatic factors and weak earthquakes may drive catastrophic rockslides disasters rather than heavy rainfall or strong earthquakes. The following conclusions can be drawn from this study:

(i) The catastrophic rockslide caused by MWBE on the eastern edge of the Tibet Plateau has large-scale characteristics, a long disaster chain, repeated occurrence and difficult prevention.
(ii) The slopes in critical regime formed by strong tectonic uplift, fast fluvial incision, high-density faults, and significant regional water confluence area laid the basis for catastrophic

rockslides. Therefore, the target rockslide-prone areas can be identified early based on the tectonic background and geomorphological characteristics.

(iii) The MWBE of early dry-heat events and antecedent rainfall, combined with imminent weak earthquakes, drive the occurrence of AGSR. Therefore, the compound of multiple small factors can be used for the prediction and warning of landslides, but its accuracy needs to be further improved with the increasing number of study cases.

(iv) The delayed amplified runoff moving toward the sliding surface and lowering of the strength of the locking-rock segment constituted the fundamental mechanism of the MWBE on catastrophic rockslide. Therefore, special attention should be paid to the hysteresis characteristics between the time of such a rockslide and peak rainfall.

CRediT authorship contribution statement

Ningsheng Chen: Conceptualization, Methodology, Investigation, Writing – original draft. **Shufeng Tian:** Conceptualization, Investigation, Writing – original draft, Writing – review & editing. **Fawu Wang:** Conceptualization, Writing – review & editing. **Peijun Shi:** Conceptualization, Writing – review & editing. **Lihong Liu:** Methodology, Software. **Miaoyuan Xiao:** Investigation. **Enlong Liu:** Writing – review & editing. **Wenqing Tang:** Writing – review & editing. **Mahfuzur Rahman:** Writing – review & editing. **Marcelo Somos-Valenzuela:** Writing – review & editing.

Declaration of Competing Interest

The authors declare that they have no known competing financial interests or personal relationships that could have appeared to influence the work reported in this paper.

Acknowledgments

We would like to thank the reviewers and the Handling Editor Prof. W.G. Zhang for their constructive comments, which substantially improved our manuscript. We also thank to the Chengdu Center of China Geological Survey for their support and help in the investigation. This research is financially supported by the National Natural Science Foundation of China (Grant No. U20A20110), the Second Tibetan Plateau Scientific Expedition and Research Program (Grant No. 2019QZKK0906), the Key R&D Projects of Tibet Autonomous Region Science and Technology Pro ject (Grant No. XZ202101ZD0013G), the International Cooperation Overseas Platform Project, CAS (Grant No. 131C11KYSB20200033) and the Outstanding Talent Project of Thousand Talents Program in China.

Appendix A. Supplementary data

Supplementary data to this article can be found online at https://doi.org/10.1016/j.gsf.2023.101627.

References

Alsharawi, Z., Angelos, J., 2006. On the periodic logistic equation. Appl. Math. Comput. 180, 342–352.
Barnard, P.L., Owen, L.A., Sharma, M.C., Finkel, R.C., 2001. Natural and human induced landsliding in the Garhwal Himalaya of Northern India. Geomorphology 40, 21–35.
Berrocal, J., Espinosa, A.F., Galdos, J., 1978. Seismological and geological aspects of the Mantaro landslide in Peru. Nature 275, 533–536.
Bevacqua, E., De Michele, C., Manning, C., Couasnon, A., Ribeiro, A.F.S., Ramos, A.M., Vignotto, E., Bastos, A., Blesić, S., Durante, F., Hillier, J., Oliveira, S.C., Pinto, J.G., Ragno, E., Rivoire, P., Saunders, K., Wiel, K., Wu, W., Zhang, T., Zscheischler, J., 2021. Guidelines for Studying Diverse Types of Compound Weather and Climate Events. Earth's Future 9, 1–23.
Bloschl, G., Hall, J., Viglione, A., Perdigao, R.A.P., Parajka, J., Merz, B., Lun, D., Arheimer, B., Aronica, G.T., Bilibashi, A., Bohac, M., Bonacci, O., Borga, M., Canjevac, I., Castellarin, A., Chirico, G.B., Claps, P., Frolova, N., Ganora, D., Gorbachova, L., Gul, A., Hannaford, J., Harrigan, S., Kireeva, M., Kiss, A., Kjeldsen, T.R., Kohnova, S., Koskela, J.J., Ledvinka, O., Macdonald, N., Mavrova-Guirguinova, M., Mediero, L., Merz, R., Molnar, P., Montanari, A., Murphy, C., Osuch, M., Ovcharuk, V., Radevski, I., Salinas, J.L., Sauquet, E., Sraj, M., Szolgay, J., Volpi, E., Wilson, D., Zaimi, K., Zivkovic, N., 2019. Changing climate both increases and decreases European river floods. Nature 573, 108–111.
Bontemps, N., Lacroix, P., Larose, E., Jara, J., Taipe, E., 2020. Rain and small earthquakes maintain a slow-moving landslide in a persistent critical state. Nat. Commun. 11, 780.
Carlini, M., Chelli, A., Vescovi, P., Artoni, A., Clemenzi, L., Tellini, C., Torelli, L., 2016. Tectonic control on the development and distribution of large landslides in the Northern Apennines (Italy). Geomorphology 253, 425–437.
Chen, Z., Yang, P., Liu, H., Zhang, W., Wu, C., 2019a. Characteristics analysis of granular landslide using shaking table model test. Soil Dyn. Earthq. Eng. 126, 105761.
Chen, Z., Zhang, Q., Chen, S., Wang, L., Zhou, X., 2019b. Evaluation of barrier lake breach floods: Insights from recent case studies in China. WIREs Water 7, e1408.
Coe, J., A.,, 2012. Regional moisture balance control of landslide motion: Implications for landslide forecasting in a changing climate. Geology 40, 323–326.
Copernicus, 2020. Climate data.
Delacourt, C., 2004. Velocity field of the "La Clapière" landslide measured by the correlation of aerial and QuickBird satellite images. Geophys. Res. Lett. 31, L15619.
Di, B., Zhang, H., Liu, Y., Li, J., Chen, N., Stamatopoulos, C.A., Luo, Y., Zhan, Y., 2019. Assessing Susceptibility of Debris Flow in Southwest China Using Gradient Boosting Machine. Sci. Rep. 9, 12532.
Dille, A., Dewitte, O., Handwerger, A.L., d'Oreye, N., Derauw, D., Ganza Bamulezi, G., Ilombe Mawe, G., Michellier, C., Moeyersons, J., Monsieurs, E., Mugaruka Bibentyo, T., Samsonov, S., Smets, B., Kervyn, M., Kervyn, F., 2022. Acceleration of a large deep-seated tropical landslide due to urbanization feedbacks. Nat. Geosci. 15, 1048–1055.
Ding, C., Feng, G., Liao, M., Tao, P., Zhang, L., Xu, Q., 2021. Displacement history and potential triggering factors of Baige landslides, China revealed by optical imagery time series. Remote Sens. Environ. 254, 112253.
Dong, J., Zhang, L., Li, M., Yu, Y., Liao, M., Gong, J., Luo, H., 2017. Measuring precursory movements of the recent Xinmo landslide in Mao County, China with Sentinel-1 and ALOS-2 PALSAR-2 datasets. Landslides 15, 135–144.
Egholm, D.L., Knudsen, M.F., Sandiford, M., 2013. Lifespan of mountain ranges scaled by feedbacks between landsliding and erosion by rivers. Nature 498, 475–478.
Fan, X., Xu, Q., Scaringi, G., Dai, L., Li, W., Dong, X., Zhu, X., Pei, X., Dai, K., Havenith, H.-B., 2017. Failure mechanism and kinematics of the deadly June 24th 2017 Xinmo landslide, Maoxian, Sichuan, China. Landslides 14, 2129–2146.
Fan, X., Xu, Q., Alonso-Rodriguez, A., Subramanian, S.S., Li, W., Zheng, G., Dong, X., Huang, R., 2019a. Successive landsliding and damming of the Jinsha River in eastern Tibet, China: prime investigation, early warning, and emergency response. Landslides 16, 1003–1020.
Fan, X., Yang, F., Siva Subramanian, S., Xu, Q., Feng, Z., Mavrouli, O., Peng, M., Ouyang, C., Jansen, J.D., Huang, R., 2019b. Prediction of a multi-hazard chain by an integrated numerical simulation approach: the Baige landslide, Jinsha River, China. Landslides 17, 147–164.
Gariano, S.L., Guzzetti, F., 2016. Landslides in a changing climate. Earth Sci. Rev. 162, 227–252.
Gu, X., Wang, L., Ou, Q., Zhang, W., 2023. Efficient stochastic analysis of unsaturated slopes subjected to various rainfall intensities and patterns. Geosci. Front. 14, 101490.
Handwerger, A.L., Roering, J.J., Schmidt, D.A., 2013. Controls on the seasonal deformation of slow-moving landslides. Earth Planet. Sci. Lett. 377–378, 239–247.
Handwerger, A.L., Rempel, A.W., Skarbek, R.M., Roering, J.J., Hilley, G.E., 2016. Rate-weakening friction characterizes both slow sliding and catastrophic failure of landslides. Proc. Natl. Acad. Sci. USA 113, 10281–10286.
Huang, R., 2009. Some catastrophic landslides since the twentieth century in the southwest of China. Landslides 6, 69–81.
Huang, Z., Law, K.T., Liu, H., Jiang, T., 2008. The chaotic characteristics of landslide evolution: a case study of Xintan landslide. Environ. Geol. 56, 1585–1591.
Huang, D., Li, Y.Q., Song, Y.X., Xu, Q., Pei, X.J., 2019. Insights into the catastrophic Xinmo rock avalanche in Maoxian county, China: Combined effects of historical earthquakes and landslide amplification. Eng. Geol. 258, 105158.
Intrieri, E., Raspini, F., Fumagalli, A., Lu, P., Del Conte, S., Farina, P., Allievi, J., Ferretti, A., Casagli, N., 2017. The Maoxian landslide as seen from space: detecting precursors of failure with Sentinel-1 data. Landslides 15, 123–133.
Iverson, R.M., George, D.L., Allstadt, K., Reid, M.E., Collins, B.D., Vallance, J.W., Schilling, S.P., Godt, J.W., Cannon, C.M., Magirl, C.S., Baum, R.L., Coe, J.A., Schulz, W.H., Bower, J.B., 2015. Landslide mobility and hazards: implications of the 2014 Oso disaster. Earth Planet. Sci. Lett. 412, 197–208.
Keefer, D.K., 1984. Landslides caused by earthquakes. Geol. Soc. Am. Bull. 95, 406–421.
Larsen, I.J., Montgomery, D.R., 2012. Landslide erosion coupled to tectonics and river incision. Nat. Geosci. 5, 468–473.
Lewkowicz, A.G., Way, R.G., 2019. Extremes of summer climate trigger thousands of thermokarst landslides in a High Arctic environment. Nat. Commun. 10, 1329.

Li, M., Zhang, L., Ding, C., Li, W., Luo, H., Liao, M., Xu, Q., 2020. Retrieval of historical surface displacements of the Baige landslide from time-series SAR observations for retrospective analysis of the collapse event. Remote Sens. Environ. 240, 111695.

Liu, X., Zhao, C., Zhang, Q., Lu, Z., Li, Z., 2020. Deformation of the Baige Landslide, Tibet, China, Revealed Through the Integration of Cross-Platform ALOS/PALSAR-1 and ALOS/PALSAR-2 SAR Observations. Geophys. Res. Lett. 47(3), e2019GL086142.

Liu, Y., Tang, W., Zhao, J., 2010. GPS monitoring of modern crustal movement in the eastern and adjacent areas of the Qinghai-Tibet Plateau. Geological Publishing House (in Chinese).

Lorenz, E.N., 1963. Deterministic nonperiodic flow. J. Atoms. 20, 130–141. https://doi.org/10.1175/1520-0469(1963)020<0130:DNF>2.0.CO;2.

May, R.M., 1976. Simple mathematical models with very complicated dynamics. Nature 261, 459–467.

Meunier, P., Hovius, N., Haines, J.A., 2008. Topographic site effects and the location of earthquake induced landslides. Earth Planet. Sci. Lett. 275, 221–232.

Moon, S., Page Chamberlain, C., Blisniuk, K., Levine, N., Rood, D.H., Hilley, G.E., 2011. Climatic control of denudation in the deglaciated landscape of the Washington Cascades. Nat. Geosci. 4, 469–473.

Olsen, R.S., Villanueva, E., 2007. Geotechnical Evalation of the Massive El Berrinche Landsile in Honduras. In: 1stNorth American Landslide Conference, AEG. Vail, Colorado, USA.

Ouyang, C., An, H., Zhou, S., Wang, Z., Su, P., Wang, D., Cheng, D., She, J., 2019. Insights from the failure and dynamic characteristics of two sequential landslides at Baige village along the Jinsha River, China. Landslides 16, 1397–1414.

Palmer, J., 2017. Creeping earth could hold secret to deadly landslides. Nature 548, 384–386.

Phillips, J.D., 1992. Nonlinear dynamical systems in geomorphology: revolution or evolution? Geomorphology 5, 219–229.

Ren, D., 2014. The devastating Zhouqu storm-triggered debris flow of August 2010: Likely causes and possible trends in a future warming climate. J. Geophys. Res. Atmos. 119, 3643–3662.

Scaringi, G., Fan, X., Xu, Q., Liu, C., Ouyang, C., Domenech, G., Yang, F., Dai, L., 2018. Some considerations on the use of numerical methods to simulate past landslides and possible new failures: the case of the recent Xinmo landslide (Sichuan, China). Landslides 15, 1359–1375.

Schneider, H., Höfer, D., Irmler, R., Daut, G., Mäusbacher, R., 2010. Correlation between climate, man and debris flow events — A palynological approach. Geomorphology 120, 48–55.

Schulz, W.H., Kean, J.W., Wang, G., 2009. Landslide movement in southwest Colorado triggered by atmospheric tides. Nat. Geosci. 2, 863–866.

Schwalm, C.R., Anderegg, W.R.L., Michalak, A.M., Fisher, J.B., Biondi, F., Koch, G., Litvak, M., Ogle, K., Shaw, J.D., Wolf, A., Huntzinger, D.N., Schaefer, K., Cook, R., Wei, Y., Fang, Y., Hayes, D., Huang, M., Jain, A., Tian, H., 2017. Global patterns of drought recovery. Nature 548, 202–205.

Shang, Y., Yang, Z., Li, L., Liu, D.a., Liao, Q., Wang, Y., 2003. A super-large landslide in Tibet in 2000: background, occurrence, disaster, and origin. Geomorphology 54, 225–243.

Shen, Z.K., Sun, J., Zhang, P., Wan, Y., Wang, M., Bürgmann, R., Zeng, Y., Gan, W., Liao, H., Wang, Q., 2009. Slip maxima at fault junctions and rupturing of barriers during the 2008 Wenchuan earthquake. Nat. Geosci. 2, 718–724.

Song, C., Yu, C., Li, Z., Utili, S., Frattini, P., Crosta, G., Peng, J., 2022. Triggering and recovery of earthquake accelerated landslides in Central Italy revealed by satellite radar observations. Nat. Commun. 13, 7278.

Su, L.-J., Hu, K.-H., Zhang, W.-F., Wang, J., Lei, Y., Zhang, C.-L., Cui, P., Pasuto, A., Zheng, Q.-H., 2017. Characteristics and triggering mechanism of Xinmo landslide on 24 June 2017 in Sichuan, China. J. Mt. Sci. 14, 1689–1700.

Tan, W., Wang, C., Yao, L., Jin, Y., Yang, W., 1994. Regional Prediction and Forecasting of Storm debris flow and landslide in Panxi Region as an Example. Sichuan Science and Technology Press. 279 pp (in Chinese.

Tian, S., Chen, N., Wu, H., Yang, C., Zhong, Z., Rahman, M., 2020. New insights into the occurrence of the Baige landslide along the Jinsha River in Tibet. Landslides 17, 1207–1216.

Turzewski, M.D., Huntington, K.W., Licht, A., Lang, K.A., 2020. Provenance and erosional impact of Quaternary megafloods through the Yarlung-Tsangpo Gorge from zircon U-Pb geochronology of flood deposits, eastern Himalaya. Earth Planet. Sci. Lett. 535, 116113.

Velasco, A.A., Hernandez, S., Parsons, T., Pankow, K., 2008. Global ubiquity of dynamic earthquake triggering. Nat. Geosci. 1, 375–379.

Wang, Z.H., Lu, J.T., 2002. Satellite monitoring of the Yigong landslide in Tibet, China. In: Conference on Earth Observing Systems VII. Spie-Int Soc Optical Engineering, Seattle, Wa, pp. 34–38.

Wang, B., Yang, S., Chen, C., 2022. Landslide dam breaching and outburst floods: A numerical model and its application. J. Hydrol. 609, 127733.

Watkinson, I.M., Hall, R., 2019. Impact of communal irrigation on the 2018 Palu earthquake-triggered landslides. Nat. Geosci. 12, 940–945.

Xiong, Z., Feng, G., Feng, Z., Miao, L., Wang, Y., Yang, D., Luo, S., 2020. Pre- and post-failure spatial-temporal deformation pattern of the Baige landslide retrieved from multiple radar and optical satellite images. Eng. Geol. 279, 105880.

Xu, Q., Shang, Y., van Asch, T., Wang, S., Zhang, Z., Dong, X., 2012. Observations from the large, rapid Yigong rock slide – debris avalanche, southeast Tibet. Can. Geotech. J. 49, 589–606.

Yi, S., Wu, C., Cui, P., Li, Y., Lei, M., Ren, T., 2022. Cause of the Baige Landslides: Long-Term Cumulative Coupled Effect of Tectonic Action and Surface Erosion. Lithosphere 2021, 7784535.

Zhang, W., Li, H., Han, L., Chen, L., Wang, L., 2022a. Slope stability prediction using ensemble learning techniques: A case study in Yunyang County, Chongqing, China. J. Rock Mech. Geotech. Eng. 14, 1089–1099.

Zhang, Y., Liu, S., Ding, Y., 2006. Observed degree-day factors and their spatial variation on glaciers in western China. Ann. Glaciol. 43, 301–306.

Zhang, W., Wu, C., Tang, L., Gu, X., Wang, L., 2022b. Efficient time-variant reliability analysis of Bazimen landslide in the Three Gorges Reservoir Area using XGBoost and LightGBM algorithms. Gondwana Res. in press. https://doi.org/10.1016/j.gr.2022.10.004.

Zhao, S., He, S., Li, X., Deng, Y., Liu, Y., Yan, S., Bai, X., Xie, Y., 2021. The Xinmo rockslide-debris avalanche: An analysis based on the three-dimensional material point method. Eng. Geol. 287, 106109.

Zhong, Z., Chen, N., Hu, G., Han, Z., Ni, H., 2021. Aggravation of debris flow disaster by extreme climate and engineering: a case study of the Tongzilin Gully, Southwestern Sichuan Province. China. Nat. Hazard. 109, 237–253.

Zhou, J.-W., Cui, P., Hao, M.-H., 2015. Comprehensive analyses of the initiation and entrainment processes of the 2000 Yigong catastrophic landslide in Tibet, China. Landslides 13, 39–54.

Zhou, S., Ouyang, C., Huang, Y., 2022. An InSAR and depth-integrated coupled model for potential landslide hazard assessment. Acta Geotech. 17, 3613–3632.

Zhou, G.G.D., Roque, P.J.C., Xie, Y., Song, D., Zou, Q., Chen, H., 2020. Numerical study on the evolution process of a geohazards chain resulting from the Yigong landslide. Landslides 17, 2563–2576.